Neurobiology of Disease 137 (2020) 104758

Contents lists available at ScienceDirect

Neurobiology of Disease

journal homepage: www.elsevier.com/locate/ynbdi

Altered excitatory transmission onto hippocampal interneurons in the IQSEC2 mouse model of X-linked neurodevelopmental disease

Megha Sah[a], Amy N. Shore[b], Sabrina Petri[a], Ayla Kanber[a], Mu Yang[a], Matthew C. Weston[b], Wayne N. Frankel[a,*]

[a] Department of Genetics & Development, Institute for Genomic Medicine, Columbia University, New York, NY 10032, United States of America
[b] Department of Neurological Sciences, University of Vermont, Burlington, VT 05405, United States of America

ARTICLE INFO

Keywords:
IQSEC2
Knockout mouse model
Epileptic encephalopathy
Seizure
Synaptic signaling
Interneurons
Behavior

ABSTRACT

Mutations in the X-linked gene *IQSEC2* are associated with multiple cases of epilepsy, epileptic encephalopathy, intellectual disability and autism spectrum disorder, the mechanistic understanding and successful treatment of which remain a significant challenge in *IQSEC2* and related neurodevelopmental genetic diseases. To investigate disease etiology, we studied behaviors and synaptic function in IQSEC2 deficient mice. Hemizygous *Iqsec2* null males exhibit growth deficits, hyperambulation and hyperanxiety phenotypes. Adult hemizygotes experience lethal spontaneous seizures, but paradoxically have a significantly increased threshold to electrically induced limbic seizures and relative resistance to chemically induced seizures. Although there are no gross defects in brain morphology, hemizygotes exhibit stark hippocampal reactive astrogliosis. Electrophysiological recordings of hippocampal neurons reveal increased excitatory drive specifically onto interneurons, and significant alterations in intrinsic electrical properties specific to the interneuron population. As they age, hemizygotes also develop an increased abundance of parvalbumin-positive interneurons in the hippocampus, neurons in which IQSEC2 is expressed in addition to the excitatory neurons. These findings point to a novel role of IQSEC2 in hippocampal interneuron synaptic function and development with implications for a class of intractable neurodevelopmental diseases.

1. Introduction

Mutations in the *IQSEC2* gene on Chromosome Xp11.22 are implicated in multiple cases of X-linked epileptic encephalopathy (XLEE) and X-linked intellectual disability (XLID). *IQSEC2* encodes a large 1488 amino acid protein with multiple functionally important domains such as the catalytic Sec 7 domain for loading GTP onto the small GTPase Arf6, a pleckstrin homology (PH) domain, a putative calmodulin binding IQ-like motif, a coiled-coiled (CC) motif and a PDZ protein binding domain (Murphy et al., 2006; Sanda et al., 2009). The IQSEC guanine exchange factor (GEF) family consists of three members - IQSEC1, IQSEC2 and IQSEC3 - proteins with non-overlapping functions. While IQSEC1 and IQSEC2 are expressed exclusively at excitatory synapses, IQSEC3 is a part of the inhibitory postsynapse (Um, 2017). The IQSEC2 protein is highly enriched in the postsynaptic density (PSD) of excitatory glutamatergic synapses where it has been shown to form protein-protein interactions with postsynaptic density (PSD) proteins such as PSD-95 (Sakagami et al., 2008), IRSp53 (Sanda et al., 2009) CamkII (Baucum et al., 2015), SAP-97 (Baucum et al., 2015) and NMDARs (Elagabani et al., 2016). Functionally, at excitatory synapses, it has been shown to carry out activity dependent removal of the AMPAR subunit GluA1 (Myers et al., 2012), insertion of AMPAR subunit GluA2 (Brown et al., 2016), mediate long term depression (Brown et al.,2016), regulate synaptic NMDAR expression (Elagabani et al., 2016) and dendritic spine development (Hinze et al., 2017). Therefore, it can be safely hypothesized that glutamatergic synapse alterations due to mutations in IQSEC2 would underlie associated behavioral and cognitive perturbations.

IQSEC2 was first linked to epileptic encephalopathy in a patient with X autosome translocation causing disruption of the *IQSEC2* gene (Morleo et al., 2008). Shortly after, a large X chromosome resequencing study revealed *IQSEC2* mutations in patients with non-syndromic X-linked intellectual disability (XLID) (Shoubridge et al., 2010a). Functional assays revealed that the identified mutations affecting conserved amino acids in the functional Sec 7 and IQ-like motif domains all suppressed IQSEC2 catalytic activity (Shoubridge et al., 2010b) Since then, there has been a surge in the number of identified clinical IQSEC2 cases. To date, over 70 pathogenic variants have been recorded, and

* Corresponding author.
E-mail address: wf2218@cumc.columbia.edu (W.N. Frankel).

https://doi.org/10.1016/j.nbd.2020.104758
Received 13 October 2019; Received in revised form 16 December 2019; Accepted 20 January 2020
Available online 21 January 2020

around 136 patients harboring *IQSEC2* mutations reported (Mignot et al., 2018; Shoubridge et al., 2019; Radley et al., 2019; Zerem et al., 2016). Commonly diagnosed IQSEC2 variant phenotype includes epilepsy, intellectual disability, developmental delay, developmental regression, autism, speech and language deficits. (Mignot et al., 2018; Zerem et al., 2016; Radley et al., 2019; Shoubridge et al., 2019). Lennox-Gastaut syndrome and Rett Syndrome-like phenotypes are also reported co-morbidities in a few patients (Olson et al., 2015; Srivastava et al., 2018; Radley et al., 2019; Zerem et al., 2016). The seizure types range from spasms to generalized tonic-clonic, and epilepsy associated with epileptic encephalopathy is pharmacoresistant (Zerem et al., 2016; Shoubridge et al., 2019; Mignot et al., 2018).

Interestingly, Mignot and colleagues (Mignot et al., 2018) report that a significant fraction of IQSEC2 pathogenic variants identified in their screen of 42 patients, 37 of which were previously undiagnosed, are predicted to end in early termination codons. These loss of function variants primarily linked to *de novo* mutations, affect both sexes and are linked to a spectrum of phenotypic severity spanning from severe intellectual disability, epileptic encephalopathy, global developmental delay, loss of speech and autism.

Despite the steady increase in these reported clinical cases, the research in animal models remains at a nascent stage. The first published report of the *Iqsec2* knockout mouse model was in 2017 (Hinze et al., 2017) in which they used hippocampal neuronal cultures from the null mice to examine IQSEC2's role in regulation of dendritic branching and morphogenesis. Earlier this year, Rogers and colleagues (Rogers et al., 2019) reported on the IQSEC2 animal model harboring a disease-causing missense mutation (A350V) in the IQ-like domain. This mutation exhibits reduced levels of AMPA receptors and autism-like behavioral perturbations. While our manuscript was in preparation, Jackson and colleagues (Jackson et al., 2019) published on the IQSEC2 mouse model which was earlier examined in the 2017 study. Here they carried out behavior and seizure phenotyping primarily of the *Iqsec2* heterozygous knockout female mice and showed that downstream Arf6 signaling pathway is altered in *Iqsec2* mutants. Additionally, they also reported a novel IQSEC2 nonsense variant c.566C > A, p.(S189*) in an elderly female patient.

Here we describe the impact of IQSEC2 deficiency on disease etiology using the *Iqsec2* knockout mouse, modeling the majority of disease variants. We observed altered seizure susceptibility, developmental and behavioral abnormalities, hippocampus-specific reactive gliosis, increased excitatory transmission onto hippocampal interneurons, and atypical expression of hippocampal fast-spiking parvalbumin interneurons. Importantly, these results outline IQSEC2 as an important regulator of *in vivo* network homeostasis, highlight a novel role in hippocampal interneuron function and suggest new pathophysiological signature in this and related childhood neurological disease.

2. Methods

2.1. Mice and genotyping

Iqsec2 knockout mice were generated using CRISPR/Cas9 at The Jackson Laboratory (Bar Harbor, ME). Briefly, a guide RNA 5'-AGCGA CTCATTGAAGCTTTCAGG-3′ was injected into single-cell mouse embryos of the C57BL/6NJ (B6NJ) inbred strain. Of 9 founder mice, one founder male carrying a 1 nt deletion in approximately 50% of somatic DNA, was bred to wildtype B6NJ females, from which the mutant colony was expanded. For optimizing fecundity and maternal care, mice were maintained on a mixed genetic background of C3HeB/FeJ x B6NJ. Male mice were used for experiments, unless stated otherwise, to avoid the confounding effects of X-inactivation in females. Genotyping was by PCR amplification and Sanger sequencing using primer pairs: Iqsec2 F: ATG GGT GTG TCA GTG GTT TGT GTA GAG, Iqsec2 R: TTG GAA CTC ACT ACA TAG ACC AGT CTG. The protein nomenclature for the frameshift mutation is p.Phe860SerfsTer8.

2.2. RNA isolation and qRT-PCR

Forebrain, cortex and hippocampus from either young or adult animals were used for RNA analysis. Isolation of total RNA with Trizol (Invitrogen, USA) was operated according to the manufacturer's protocol with minor modifications and qRT-PCR performed with an Applied Biosystems- Quant Studio5.

RT-PCR primers.

Rpl13.

F: AGCCGGAATGGCATGATACTG.

R: TATCTCACTGTAGGGCACCTC.

Pvalb.

F: TGTCGATGACAGACGTGCTC.

R: TTCTTCAACCCCAATCTTGC.

Sst

F: ACCGGGAAACAGGAACTGG.

R: TTGCTGGGTTCGAGTTGGC.

Iqsec2.

5' CTTCATCCTGGAGAGGAAAGG 3′.

5' CACTGGGGCTGTACATATCG 3'.

Iqsec1.

F: AGTCCAGACCACTACGAGCA.

R: TGCGTTCTAGCATTTCCACCT.

Iqsec3.

F: CACCATTCAAACCGCTTTTCG.

R: CACCAGACTCTCCGCTGTG.

2.3. Western blotting

To evaluate protein levels, protein extracts were prepared as described from dissected forebrain and hippocampal tissue (Murphy et al., 2006). Primary antibodies: IQSEC2 (N-terminus antibody- 1:100; antiserum UCT 88, a gift from Dr. Randall Walikonis recognizes residues 10–198 of human IQSEC2) and AB_2718685 (C-terminus antibody 1:50; Invitrogen recognizes residues 1380–1430 of human IQSEC2), guinea pig anti-parvalbumin-α (1:1000; Synaptic Systems, Cat# 195004), rabbit anti-IQSEC1 (1:500 Biorybt, cat# orb183807), rabbit anti-IQSEC3(1:500, Thermo Fisher, cat# PA5–25866) anti-glial fibrillary acid protein (GFAP; 1:750; Sigma-Aldrich, Cat# G3893), mouse anti-tubulin (1:2000; Biolegend, Cat# 903401). Signal was detected with corresponding HRP-conjugated secondary antibodies and Immobilon Western Chemiluminescent HRP substrate (Millipore).

2.4. Immunofluorescence

Two methods were used for IHC since the IQSEC2 serum antibodies do not work with perfused tissue: Flash-frozen sections (IQSEC2, PV together); PFA perfused sections (PV only). Primary antibodies: rabbit anti-IQSEC2 [1:100; antiserum UCT 88,(Murphy et al., 2006)], chicken anti-IQSEC2 [1:50; antiserum UCT C3(Murphy et al., 2006),guinea pig anti-parvalbumin-α [1:1000; Synaptic Systems, Cat# 195004], and anti-glial fibrillary acid protein (GFAP) antibody (1:750; Sigma-Aldrich, Cat# G3893). Secondary antibodies: Alexa Fluor 488-conjugated goat anti-mouse, 568-conjugated goat anti-rabbit, and Alexa Fluor 647-conjugated goat anti-chicken IgG (1:500 in blocking buffer; Invitrogen) and Alexa Fluor 555-conjugated goat anti-guinea pig (1:500 in blocking buffer; Abcam).

Parvalbumin immunoreactive neurons were imaged using an automated slide-scanner (Zeiss LSM-800 confocal microscope and Zen v2.3). In a blind study, total counts of parvalbumin immunoreactive cells were made from 3 sections per animal from the left hemisphere using ImageJ (v1.46), from dorsal hippocampus separated into the CA1, CA3 and DG regions. The total counts for the hippocampus included the subiculum. Regions were delineated using clearly visible landmarks and predefined boundaries according to the Allen Brain Atlas.

2.5. Dentate gyrus measurement

We used Cavalieri's principle, which allows obtaining an estimated volume of an object of arbitrary shape and size to measure thickness of the granule cell layer of the supra pyramidal blade. The following formula was used:

$$V = T * \sum (i = 1 - - > n)A$$

where V is the volume, T the distance between parallel sections, A the calculated area of a section, and n the total number of sections. 3 region matching sections between the genotypes were measured every 15 μm.

2.6. Cell culture for electrophysiology

To generate astrocyte feeder layers, cortical hemispheres from postnatal day 0–1 (PND0–1) wildtype C57BL/6 J mice of either sex were dissected in cold HBSS (Gibco). For primary neuron culture, hippocampi from PND1–2 mice were dissected in cold HBSS and cell culture carried out as described (Weston et al., 2014). The day after plating, approximately 4×10^{10} genome copies of AAV8-CaMKII-GFP virus (UNC Vector Core) was added to each well.

2.7. Electrophysiology

Whole-cell recordings were performed with patch-clamp amplifiers (MultiClamp 700B amplifier; Molecular Devices) under the control of Clampex 10.3 or 10.5 (Molecular Devices, pClamp, RRID:SCR_011323). Data were acquired at 10 kHz and low-pass filtered at 6 kHz. The series resistance was compensated at 70%, and only cells with series resistances maintained at < 15 MΩ were analyzed. Patch electrodes were pulled from 1.5-mm o.d. thin-walled glass capillaries (Sutter Instruments) in five stages on a Flaming–Brown micropipette puller (model P-97; Sutter Instruments). Internal solution contained the following: 136 mM KCl, 17.8 mM HEPES, 1 mM EGTA, 0.6 mM MgCl2, 4 mM ATP, 0.3 mM GTP, 12 mM creatine phosphate, and 50 U/ml phosphocreatine kinase. The pipette resistance was between 2 and 4 MΩ. Standard extracellular solution contained the following (in mM): 140 NaCl, 2.4 KCl, 10 HEPES, 10 glucose, 4 MgCl2, and 2 CaCl2 (pH 7.3, 305 mOsm). All experiments were performed at room temperature (22–23 °C). Whole-cell recordings were performed on neurons from *Iqsec2*$^{-/Y}$ and wildtype groups in parallel on the same day (day 12–15 *in vitro*). On each day, and for each group, an attempt was made to record from equal numbers of glutamatergic (GFP^+) and GABAergic (GFP^-) neurons. All electrophysiology experiments were performed by two independent investigators blinded to the genotypes, and all data were analyzed offline with AxoGraph X software (AxoGraph Scientific, RRID:SCR_014284). From a total of five cultures, we recorded from a total of 52 glutamatergic and 53 GABAergic wildtype neurons, and 54 glutamatergic and 56 GABAergic mutant neurons. From all five cultures, we recorded from a total of 34 wildtype *E*-I neuron pairs, and 32 mutant E-I neuron pairs.

For voltage-clamp experiments, neurons were held at −70 mV. Miniature synaptic potentials were recorded for 70–90 s in 500 nM tetrodotoxin (TTX, Enzo Life Sciences) to block AP-evoked release, and either the $GABA_A$ receptor antagonist bicuculine methiodide (30 μM; hello bio) to isolate mEPSCs, or the AMPA receptor antagonist NBQX disodium salt (10 μM; TOCRIS Bioscience) to isolate mIPSCs. Data were filtered at 1 kHz and analyzed using template-based miniature event detection algorithms implemented in the AxoGraph X 1.6 software. The threshold for detection was set at 3.5 times the baseline SD from a template of 0.5 ms rise time and 3 ms decay for mEPSCs, and 20 ms decay for mIPSCs. For paired neuron recordings, action potential (AP)-evoked EPSCs and IPSCs were triggered by a 2 ms somatic depolarization to 0 mV at 0.1 Hz. The shape of the evoked response and the effect of receptor antagonists (bicuculline and NBQX) were analyzed to verify the glutamatergic or GABAergic identities of the responses.

For current-clamp experiments, intrinsic electrophysiological properties of neurons were tested by injecting 500-ms square current pulses incrementing in 20 pA steps, starting at −100 pA. Resting membrane potential (Vm) was calculated from a 50 ms average before current injection. The membrane time constant (τ) was calculated from an exponential fit of current stimulus offset. Input resistance was calculated from the steady state of the voltage responses to the hyperpolarizing current steps. Membrane capacitance was calculated by dividing the time constant by the input resistance. APs were evoked with 500 ms, 20 pA depolarizing current steps, and the rheobase was defined as the minimum current required to evoke an AP during the 500 ms of sustained somatic current injections. The AP threshold was defined as the membrane potential at the inflection point of the rising phase of the AP. The AP amplitude was defined as the difference in membrane potential between the AP peak and the threshold, and the afterhyperpolarization was the difference between AP threshold and the lowest point of hyperpolarization. The AP half-width was defined as the width of the AP at half-maximal amplitude. The membrane potential values were not corrected for the liquid junction potential.

2.8. Seizure testing

For the PTZ test, adult mice between 9 and 12 weeks of age were injected subcutaneously with a threshold dose (50 mg/kg) of PTZ (Sigma-Aldrich, Co), placed onto clean bedding in a clear plastic box, and observed for 30 min. The incidence and latency to seizure endpoint standards (Racine, 1972) were recorded, and the group mean latency to tonic-clonic seizures was determined. The 6 Hz electroconvulsive threshold (ECT) test was as described previously with minor modifications (Frankel et al., 2001), was performed once daily with increasing stimulus until a partial seizure was observed. Group means were calculated to determine threshold. For video-EEG, adult mice were anesthetized and electrode implant surgery was performed as recently described (57).

2.9. Pup developmental milestones

Developmental milestones were assessed every other day starting at PND4 through PND10 (Yang et al., 2012). To avoid circadian rhythm-induced variability, each test litter was examined during the same 1 h window. To assess physical development, pups were weighed; for righting reflex, the pups were turned on their back and given 30 s to right themselves. To observe isolation-induced USV, pups were removed from their nest and isolated from mother and littermates. Pups were placed gently into a small isolation container made of plastic, containing fresh bedding material and USVs recorded using UltraSoundGate Condenser Microphone CM 16 (Avisoft Bioacoustics, Berlin, Germany). Each recording was carried out for 3 min and the number of calls emitted by the pups counted by an operator blinded to genotype.

2.10. Adult behavior

For the open field test, adult *Iqsec2* mice (8–12 weeks) were placed in the center of an acryliopen-field box and allowed to freely explore the environment for 60 min under the light condition of 10 lx. Ethovision XT software (Noldus) was used to determine distinct features of locomotor activity. For the elevated plus-maze test, the elevated plus-maze system by Med Associates Inc. (Fairfax, VT) was used. Light conditions for the test was 30 lx. In the test, mice were introduced to the center region of the elevated plus-maze and allowed to explore freely for 5 min. Male-female social interactions were evaluated in a 5-min test session as previously described (Yang et al., 2012)

2.11. Statistics

Statistical analysis was performed using GraphPad Prism 7 software. Unpaired two-tailed Student's *t*-test for parametric data and Mann–Whitney test for non-parametric data was used to detect genotype differences in immunofluorescence intensity, mRNA and protein expression, elevated maze plus times, adult USV counts and 6 Hz test thresholds. 2-way ANOVA with Sidak's multiple comparison test as a post-hoc analysis was used to analyze developmental milestones, pup ultrasonic vocalizations, righting reflex across days and adult open field data across 1 h recording time. A log-rank Mantel-Cox test was performed to compare the Kaplan–Meier analysis for adult mortality and the fisher's exact test for PTZ seizure latency. For electrophysiology data, we used generalized estimating equations (GEE) in SPSS V24 (IBM, RRID:SCR_002865), allowing for within-subject correlations and the specification of the most appropriate distribution for the data. All data distributions were assessed with the Shapiro-Wilk test. Datasets that were significantly different from the normal distribution ($p < .05$) were fit with models using the gamma distribution and a log link. Normal datasets were fit with models using a linear distribution and identity link. We used the model-based estimator for the covariance matrix and an exchangeable structure for the working correlation matrix. Goodness of fit was determined using the corrected quasi likelihood under independence model criterion and by the visual assessment of residuals. Because neurons and animals from the same culture are not independent measurements, culture was used as the subject variable, and animals and neurons were considered within-subject measurements. All values reported in the text are estimated marginal means +/− standard error.

3. Results

3.1. Validation of the Iqsec2 knockout model

To model loss-of-function *IQSEC2* disease, we created an *Iqsec2* knockout mouse on the C57BL/6NJ (B6NJ) strain background using CRISPR/Cas9, resulting in a single nucleotide deletion and translational frameshift (p.Phe860SerfsTer8) in *Iqsec2* exon 7 (Fig. 1A). Because hemizygous *Iqsec2*$^{-/Y}$ males do not mate well, and on the B6NJ background heterozygous females are inattentive to pups, all studies were performed on a mixed hybrid background involving the C3HeB/FeJ and C57BL/6NJ strains. To detect *Iqsec2* gene expression, RNA primers spanning exon 6 to exon 8 were designed. RT-PCR showed lack of amplification in the *Iqsec2*$^{-/Y}$ animals compared to the wildtype littermates (Fig. 1B). To investigate protein expression, we used forebrain homogenates from postnatal day (PND) 21 animals and probed for IQSEC2 using a N-terminus antibody (UCT 88 was developed against residues 10–198 of human IQSEC2 (Murphy et al., 2006) and a C-terminus antibody (AB_2718685 recognizes residues 1380–1430 of human IQSEC2). Western blotting showed lack of protein expression and no evidence of truncated protein expression with either antibody (Fig. 1C). This evidence suggests that the premature stop codon in exon 7 subjects the mutant *Iqsec2* mRNA to nonsense mediated decay. The N-terminus antibody was used for all subsequent experiments and data presented.

To examine whether the *Iqsec2* point mutation impacts expression of IQSEC family members, namely IQSEC1, IQSEC2, and IQSEC3 we evaluated respective mRNA transcripts from forebrain samples of PND14 mutants and controls by RT-qPCR and protein levels using western blot at PND21. Compared to wildtype littermates, hemizygous males showed an approximate 40-fold decrease in *Iqsec2* mRNA expression with no change in either *Iqsec1* or *Iqsec3* mRNA expression (Fig. 1D). Western blotting confirmed unchanged protein expression for IQSEC1 and IQSEC3 in *Iqsec2*$^{-/Y}$ animals and complete absence of IQSEC2 protein (Fig. 1E), confirming specificity of *Iqsec2* targeting and importantly that the hemizygous mutant males are null for the *Iqsec2* allele.

3.2. Increased adulthood mortality in Iqsec2$^{-/Y}$ animals

Although *Iqsec2* heterozygotes and hemizygotes were born in the expected Mendelian ratio and had no overt signs of neurological deficits, they had increased mortality compared to wildtype littermates. *Iqsec2*$^{-/Y}$ mice had a median lifespan of 95 days and did not survive past 187 days (Fig. 1F). Despite showing no evidence of seizure activity during regular handling, post-mortem examination of all *Iqsec2*$^{-/Y}$ animals revealed retracted forelimbs and extended hindlimbs, suggestive of a maximal tonic seizure (Supplementary File -IQSEC2 KO Lethal Seizures -uploaded for reviewers only). Generalized tonic-clonic and maximal tonic seizures were captured live in several mice during long-term video monitoring, with hemizygotes observed suddenly breaking into a wild run followed by a terminal seizure. (Supplementary File -IQSEC2 KO Lethal Seizures -uploaded for reviewers only).

3.3. Decreased susceptibility to induced seizures in Iqsec2$^{-/Y}$ animals

To check for the presence of non-convulsive seizures or interictal epileptiform activity, continuous 48 h video-EEG was recorded from three *Iqsec2*$^{-/Y}$ and two littermate control 9-week old adult mice (Supplementary Fig. 1B). We also evaluated longer-term recordings in four *Iqsec2*$^{-/Y}$ mice between 60 and 110 days of age for a total of 96 h. No indication of any epileptiform activity was detected in these 7 mice. We do note, however, that during the final stages of preparation of our manuscript, a new publication by Jackson and colleagues reported recording spontaneous seizure activity in some adult *Iqsec2*$^{-/Y}$ animals during continuous live-video surveillance (Jackson et al., 2019). We suspect that differences in the respective strain background, or in the animal care environment, impact the manifestation of recurrent (non-lethal) spontaneous seizures.

To gain further insight into network excitability, we examined threshold to induced seizures using the 6 Hz electroconvulsive threshold (ECT) test and the pentylenetetrazole (PTZ) chemoconvulsion test. The 6 Hz ECT induces partial or “psychomotor” seizures and in particular is considered to be useful for studying pharmacoresistant epilepsy of limbic origin. Surprisingly and counterintuitively, compared wildtype (12.21 ± 0.5548 mA, $n = 7$), *Iqsec2*$^{-/Y}$ animals had a significantly elevated threshold to 6 Hz ECT (18.69 ± 0.4002 mA, $n = 8$, $p = .0002$; Fig. 1G). Even heterozygous *Iqsec2* mutant females had an elevated 6 Hz threshold (15.39 ± 0.535 mA, $n = 14$), in between the threshold for the wildtype controls and knockout animals (Supplementary Fig. 1A), consistent with what might be expected from random Chr X inactivation. Similarly, in the chemoconvulsion test, using a dose of PTZ at the threshold for generalized tonic-clonic seizures (GTCS) in this mixed strain background, compared to all of the control animals ($n = 10$), only 2 of the 14 *Iqsec2*$^{-/Y}$ animals experienced GTCS ($p < .0001$). Furthermore, those 2 *Iqsec2*$^{-/Y}$ mice showed increased latency to GTCS compared to the wildtype (Fig. 1H). Together, these results indicate that the susceptibility to some forms of induced seizures is actually suppressed in *Iqsec2*$^{-/Y}$ mice.

3.4. Developmental and adult behavioral deficits in Iqsec2$^{-/Y}$ animals

Patients harboring *IQSEC2* variants present a wide spectrum of phenotypes beyond seizures, including developmental regression, language development delay, intellectual disability and ASD. To test related functionality in *Iqsec2* null mice, we performed a battery of neurobehavioral tests to assess development trajectory and adult behavior.

For developmental milestones (Fig. 2A), *Iqsec2*$^{+/Y}$ ($n = 16$) and *Iqsec2*$^{-/Y}$ (n = 10) pups were assessed, with observer blind to genotype, every other day from PND4–10 for weight gain and neurological reflex including righting reflex and maternal separation-induced ultrasonic vocalization (USV). An overall genotype difference was observed in pup growth ($F_{(1, 24)} = 12.89$, $p = .0015$), whereby *Iqsec2*$^{-/Y}$ pups grew more

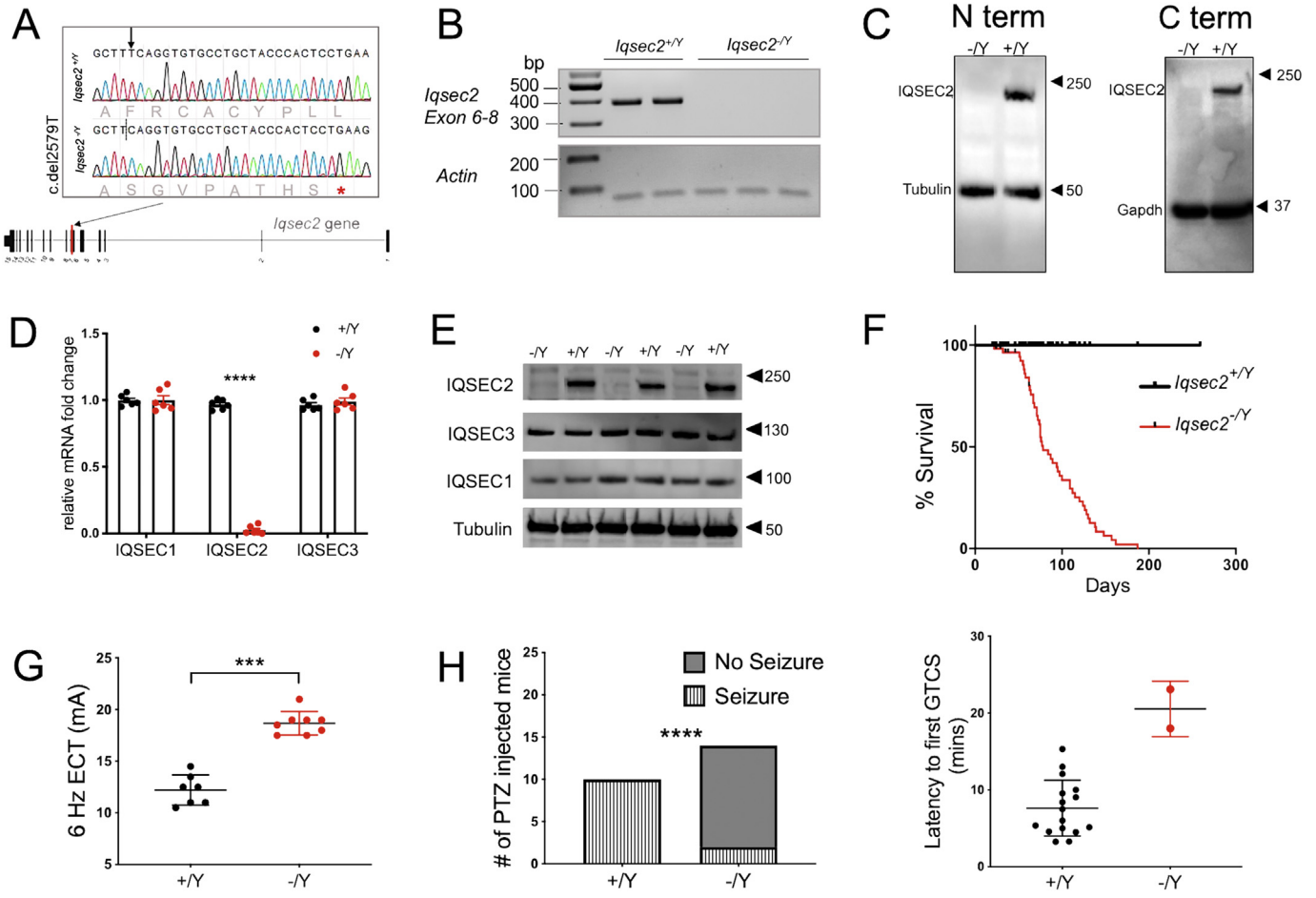

Fig. 1. Generation and characterization of *Iqsec2* mutant mice.

A. Illustration describing the location of the point mutation on exon 7 of the longest coding *Iqsec2* isoform NM_0011111125. An asterisk denotes the stop codon introduced by a frameshift due to deletion of the T nucleotide at position 2579. B. Semi quantitative RT-PCR analysis shows no amplification of exon 6–8 in the *Iqsec2*$^{+/Y}$ animals. C. Western blot showing staining for IQSEC2 and tubulin using 50 micrograms of whole brain lysate from P21 animals from each genotype using a N-terminus and C-terminus antibody shows a lack of IQSEC2 protein expression in the null animals. D. Quantitative analysis of the *Iqsec1* and *Iqsec2* mRNA transcript expression from whole brain of P14 *Iqsec2*$^{+/Y}$ and *Iqsec2*$^{-/Y}$ animals. *Iqsec1* transcript expression is unaltered between *Iqsec2*$^{+/Y}$ (0.977 ± 0.015) and *Iqsec2*$^{-/Y}$ (0.993 ± 0.64) animals, *Iqsec3* transcript expression is unaltered between *Iqsec2*$^{+/Y}$ (0.965 ± 0.017) and *Iqsec2*$^{-/Y}$ (0.990 ± 0.065) animals, whereas *Iqsec2* transcript expression is significantly reduced in *Iqsec2*$^{-/Y}$ (0.046 ± 0.023) animals compared to control *Iqsec2*$^{+/Y}$ (0.963 ± 0.20) animals, 5 animals per genotype, $p < .0001$ E. Western blot showing staining for IQSEC1, IQSEC2 (N-terminus antibody), and IQSEC3 using 50 micrograms of whole brain lysate from P21 animals from each genotype ($n = 3$ for each genotype) shows no difference in IQSEC1 and IQSEC3 expression in *Iqsec2*$^{-/Y}$ animals. F. Monitoring survival of littermate mice revealed a markedly shortened lifespan of *Iqsec2*$^{-/Y}$ ($n = 62$; median survival = 95 days) compared to *Iqsec2*$^{+/Y}$ ($n = 51$) mice, log-rank Mantel Cox test, $p < .0001$ G. Seizure thresholds are significantly different for the 6 Hz electroconvulsive test between the *Iqsec2*$^{+/Y}$($n = 7$) and *Iqsec2*$^{-/Y}$($n = 8$) animals (12.21 ± 0.5548 mA; 18.69 ± 0.4002 mA, respectively); Mann Whitney *U* test, *** $p = .0002$; error bars indicate ± SEM. H. Significantly decreased GTCS incidence in *Iqsec2*$^{-/Y}$ mice ($n = 14$) compared to *Iqsec2*$^{+/Y}$ mice ($n = 10$) after 50 mg/kg PTZ, $p < .0001$ by contingency $\chi 2$ analysis. The *Iqsec2*$^{-/Y}$ mice that exhibited GTCS on PTZ administration had a longer latency compared to the *Iqsec2*$^{+/Y}$ mice.

slowly than wildtype littermates, first apparent at PND8 (PND4 $p = .6495$, PND6 $p = .08$, PND8 $p = .001$, PND10 $p < .0001$). No significant difference between genotypes was found for righting reflex ($F_{(1, 24)} = 0.03721$, $p = .8487$) or for separation-induced USV ($F_{(1, 24)} = 0.02588$, $p = .8754$). Additionally, the *Iqsec2*$^{-/Y}$ adult animal growth never catches up to wildtype littermates (Supplementary Fig. 2A), although the weight difference becomes less statistically significant with age (PND21 $p < .0001$, PND60 $p = .09$).

For adult behaviors, 8–12 week-old *Iqsec2*$^{-/Y}$ and wildtype male littermates were assessed in the open field arena (Fig. 2B), revealing a significant increase in ambulatory activity as measured by total distance traveled over a 60 min period ($F_{(1, 28)} = 13.77$, $p = .001$), but no difference was observed in time spent in the center (Supplementary Fig. 3) ($F_{(1, 28)} = 2.173$, $p = .1516$).

We also tested the animals for anxiety-related behavior using the elevated plus-maze test (Fig. 2C). Overall, *Iqsec2*$^{-/Y}$ mice spent significantly more time in the closed arms ($p = .024$) and reciprocally, less time in the open arms ($p = .001$) than wildtype littermates. These behaviors suggest anxiety in mature *Iqsec2* null mice. Adult males typically display USV upon initiating courtship or marking their territory. Despite having viable sperm (based on successful cryopreservation), adult *Iqsec2*$^{-/Y}$ mice did not successfully mate in our hands. Therefore, we measured female-induced USV in male hemizygotes at 9–11 weeks of age, as an analogous approach to assess social and verbal communication skills (Fig. 2D). Similar measurement techniques have been frequently deployed in study of animal models with neurological deficits such as ASD (Yang et al., 2012). For this test, male *Iqsec2*$^{-/Y}$ and wildtype littermates were paired with unfamiliar estrous B6NJ females in a testing cage for a total of 5 min and the total number of calls emitted by the male mice quantified. Compared to wildtype counterparts, *Iqsec2*$^{-/Y}$ males emitted significantly fewer ultrasonic vocalizations ($p < .0001$), strongly suggesting that loss of *Iqsec2* impairs social

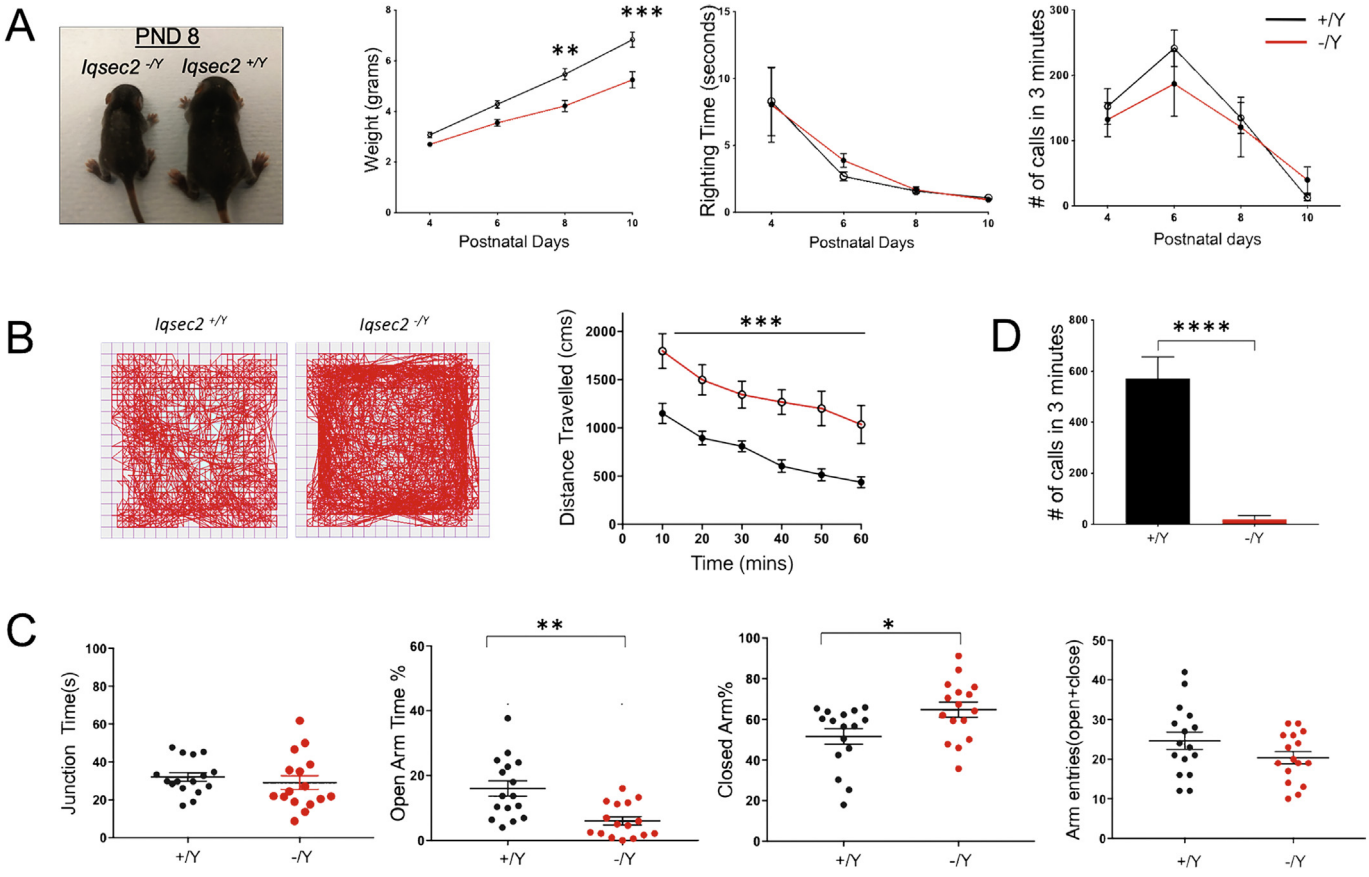

Fig. 2. Mouse pup and adult behavioral phenotyping of *Iqsec2*$^{-/Y}$ animals.
A. Panels from left to right show comparison of *Iqsec2* pups at PND8 and graphs for developmental milestones. Analysis of developmental milestone markers revealed genotype differences on measures of body weight but not righting reflex. Number of ultrasonic vocalizations emitted by pups separated from the nest did not differ significantly among genotypes but were fewer in *Iqsec2*$^{-/Y}$ mice (n = 10) compared to *Iqsec2*$^{+/Y}$ mice (n = 16); Two-way ANOVA, Sidak's multiple comparison test, $^{**}p < .01$, $^{***}p < .001$; error bars indicate ± SEM. Adult IQSEC2 animals are hyperambulatory (B), hyperanxious (C) and display defects in social interaction (D). B. Representative tracks of *Iqsec2*$^{+/Y}$ and *Iqsec2*$^{-/Y}$ mice during a 60-min open field session and graph showing total distance traveled (cms) measured in 10-min time bins across a 60-min session in an open field box, *Iqsec2*$^{+/Y}$ (n = 16) and *Iqsec2*$^{-/Y}$ (n = 14), Two-way ANOVA, $^{***}p < .001$; error bars indicate ± SEM. C. Time spent in junction, percent time spent in open arms, percent time spent in closed arms and total number of open and closed arm entries by *Iqsec2*$^{+/Y}$ (n = 16) and *Iqsec2*$^{-/Y}$ (n = 14) mice during 5 min exploration in elevated plus maze. Mann Whitney U test $^{*}p < .05$, $^{**}p < .01$; error bars indicate ± SEM. D. Total number of USV calls emitted by *Iqsec2*$^{+/Y}$ (n = 10) and *Iqsec2*$^{-/Y}$ (n = 12) mice when introduced to a novel estrous female during a social interaction session; Mann Whitney U test, $^{****}p < .0001$; error bars indicate ± SEM.

male-female interaction.

3.5. IQSEC2 protein expression and reactive astrogliosis in Iqsec2$^{-/Y}$ animals

Although evidence for *Iqsec2* mRNA localization within the brain exists (Sanda et al., 2009), protein had not been previously examined *in situ*. Temporal expression patterns demonstrate that the IQSEC2 protein is first detected at PND7 and reaches peak stable expression at PND14 (Elagabani et al., 2016b). Therefore, to obtain a snapshot of spatial protein expression we probed sagittal sections from *Iqsec2*$^{+/Y}$ and *Iqsec2*$^{-/Y}$ animals at PND16 with a serum antibody against IQSEC2 (Murphy, 2006). Consistent with previously reported forebrain mRNA expression (Sanda et al., 2009) IQSEC2 expression was highest in the hippocampal formation (Fig. 3A–B), suggesting functional importance in the region. To note, staining was completely absent from sections from *Iqsec2*$^{-/Y}$ animals, confirming antibody specificity.

Characterization of general brain architecture by Nissl staining did not reveal obvious abnormalities nor were any differences detected in brain to body weight ratio in the *Iqsec2*$^{-/Y}$ mice (Supplementary Fig. 2B-E). Double immunostaining for cleaved caspase 3, GFAP, and in parallel FluoroJade C (FJC) was performed to ascertain degenerating cells or overt cell death – both were negative. However, there was significantly increased GFAP immunoreactivity, a proxy for reactive astrogliosis, in *Iqsec2*$^{-/Y}$ hippocampal region compared to control in PND28 animals (*Iqsec2*$^{-/Y}$ N = 5, *Iqsec2*$^{+/Y}$ N = 7; Fig. 3C-E). Quantification by western blot confirmed the increase in GFAP protein expression in *Iqsec2*$^{-/Y}$ hippocampal lysate (N = 3 for each genotype); $p < .05$; Fig. 3E). In this study, we confined our examinations to the hippocampus since high protein expression and region-specific reactive astrogliosis in the knockout mice underscored both the functional relevance and therefore, the vulnerability of this region to IQSEC2 loss.

3.6. Loss of Iqsec2 enhances spontaneous and evoked glutamatergic strength onto GABAergic hippocampal neurons

Given the localization of IQSEC2 at the excitatory postsynaptic density, it is not surprising that previous studies showed that it regulates glutamatergic synaptic transmission. More specifically, one group showed that *Iqsec2* knockdown reduces, and *Iqsec2* overexpression increases, evoked excitatory postsynaptic current (eEPSC) amplitude onto CA1 pyramidal neurons of PND5–PND6 rats (Brown et al., 2016), whereas another reported that *Iqsec2* knockdown reduces the frequency of miniature excitatory postsynaptic currents (mEPSCs)

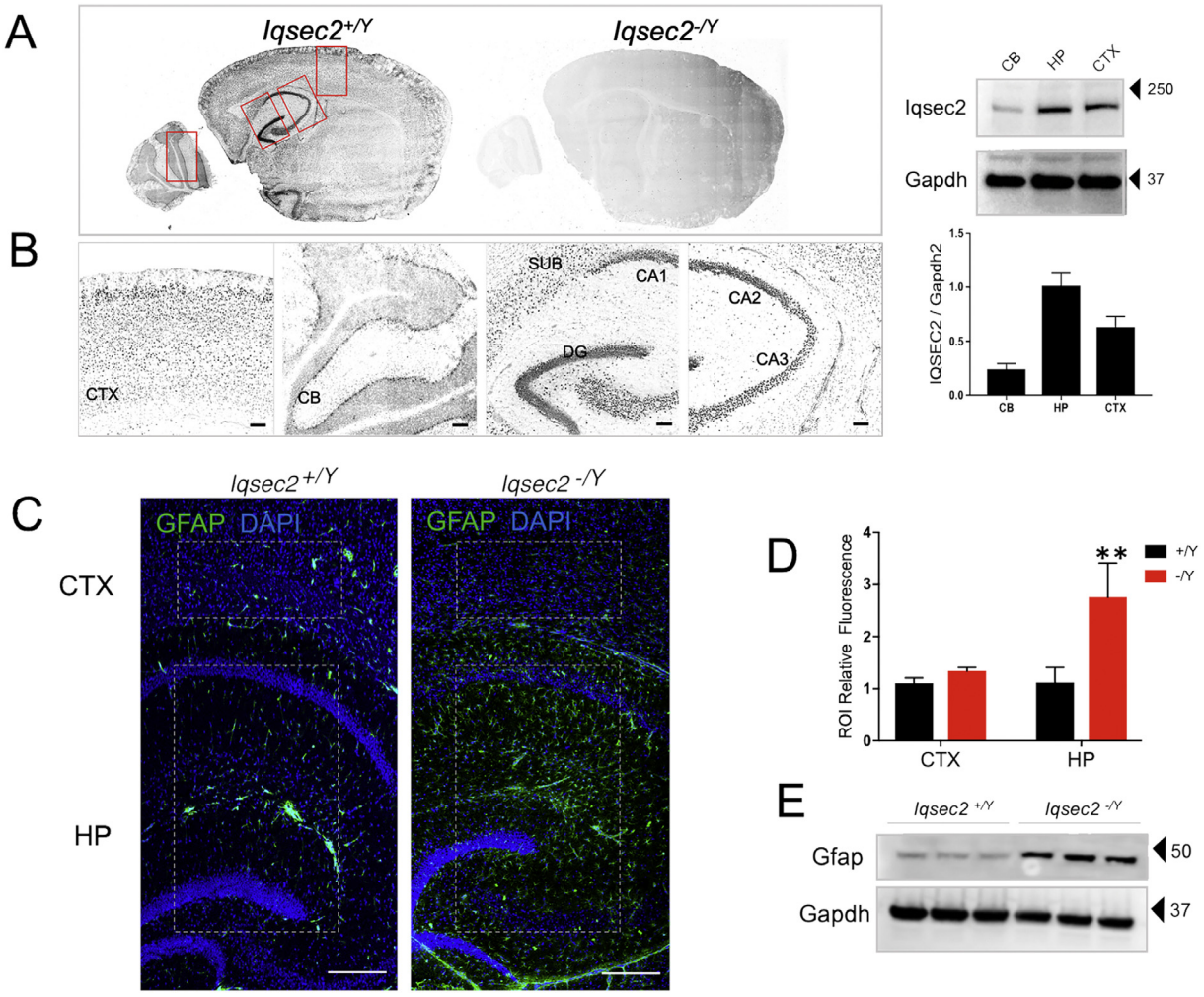

Fig. 3. IQSEC2 expression and reactive gliosis in the hippocampus.
A. Sagittal sections of PND21 mice stained with antibody against IQSEC2 (antiserum UCT88). Staining is present in *Iqsec2*$^{+/Y}$ (n = 5 animals) sections and absent from *Iqsec2*$^{-/Y}$ (*n* = 4 animals) sections confirming lack of protein expression. B. The boxed regions in panel A were zoomed in to show staining in the cortex, cerebellum and hippocampus. Expression pattern revealed increased staining in the hippocampus including CA1, CA2, CA3, dentate gyrus and subiculum. Scale bar is 20 μm. Western blot run with 50 micrograms of protein loaded from cerebellar, hippocampal and cortical lysates from a PND28 *Iqsec2*$^{+/Y}$ brain and stained against IQSEC2 and loading control GAPDH. Graph shows IQSEC2 expression normalized to input, n = 3; Error bars represent standard deviation of the mean value. C. Representative sections show that astrogliosis is absent in adult *Iqsec2*$^{+/Y}$ sections (n = 5 mice) but present and confined to the hippocampus in *Iqsec2*$^{-/Y}$ sections (n = 7 mice). Scale bars: 200 μm. Boxed regions in Panel A indicate region of interest (ROI) used for immunofluorescence quantification. D. Graph shows quantification of ROI-specific GFAP fluorescence for cortex and hippocampus compared between the genotypes. Mann Whitney U test, $^{**}p < .01$; error bars indicate ± SEM E. Western blot shows 50 μg of hippocampal lysate from 3 individual animals from each genotype (PND45–60) probed against GFAP and loading control GAPDH.

onto CA1 pyramidal neurons of PND16 mice (Elagabani et al., 2016). To determine whether IQSEC2 genetic loss alters synaptic transmission in hippocampal neurons, we generated dissociated hippocampal neuron cultures from PND1– PND2 *Iqsec2*$^{-/Y}$ and wildtype littermate pups. The cultured neurons were transfected with an adeno-associated virus expressing an enhanced green fluorescent protein driven by a calcium/calmodulin-dependent kinase II promoter (AAV-CamKII-EGFP) to better distinguish between glutamatergic and GABAergic neurons. Between 12 and 15 days *in vitro* (DIV), we performed whole-cell patch-clamp electrophysiology to assess alterations in synaptic transmission.

First, we performed voltage-clamp recordings to analyze spontaneous miniature activity onto glutamatergic and GABAergic neurons from each group. To obtain miniature activity, we recorded from neurons in a solution containing tetrodotoxin (TTX; 500 nM) and either bicuculine (30 μM) to isolate mEPSCs, or NBQX (10 μM) to isolate miniature inhibitory postsynaptic currents (mIPSCs). In contrast to previous reports, we observed no statistically significant difference in mEPSC frequency or amplitude onto *Iqsec2*$^{-/Y}$ glutamatergic neurons compared with wildtype (WT: 1.96 ± 0.18 Hz, *Iqsec2*$^{-/Y}$: 1.63 ± 0.15 Hz, $p = .17$; Fig. 4A$_{1,2}$ and WT: 10.2 ± 0.4 pA, *Iqsec2*$^{-/Y}$: 9.4 ± 0.4 pA, $p = .19$; Fig. 4A$_{1,3}$). However, there were significant increases in mEPSC frequency and amplitude onto *Iqsec2*$^{-/Y}$ GABAergic neurons compared with wildtype (WT: 5.74 ± 0.5 Hz, *Iqsec2*$^{-/Y}$: 7.58 ± 0.7 Hz, $p = .038$; Fig. 4B$_{1,2}$ and WT: 15.3 ± 0.6 pA, *Iqsec2*$^{-/Y}$: 17.3 ± 0.7 pA, $p = .017$; Fig. 4B$_{1,3}$). There were no genotype-dependent differences in mIPSCs onto glutamatergic (WT: 2.38 ± 0.2 Hz, *Iqsec2*$^{-/Y}$: 2.26 ± 0.2 Hz, $p = .65$; Supplementary Fig. 4A$_{1,2}$ and WT: 17.8 ± 1.4 pA, *Iqsec2*$^{-/Y}$: 16.9 ± 1.3 pA, $p = .45$; Supplementary Fig. 4A$_{1,3}$) or GABAergic neurons (WT: 2.72 ± 0.2 Hz, *Iqsec2*$^{-/Y}$: 3.10 ± 0.3 Hz, $p = .25$; Supplementary Fig. 4B$_{1,2}$ and WT: 18.8 ± 1.5 pA, *Iqsec2*$^{-/Y}$: 18.3 ± 1.4 pA, $p = .71$; Supplementary Fig. 4B$_{1,3}$).

To determine whether the enhanced spontaneous glutamatergic transmission onto GABAergic neurons also occurs upon evoked release, we performed paired recordings of glutamatergic and GABAergic neurons from *Iqsec2*$^{-/Y}$ and wildtype hippocampal neuron cultures (DIV 12–15). For each pair, we stimulated a glutamatergic neuron and

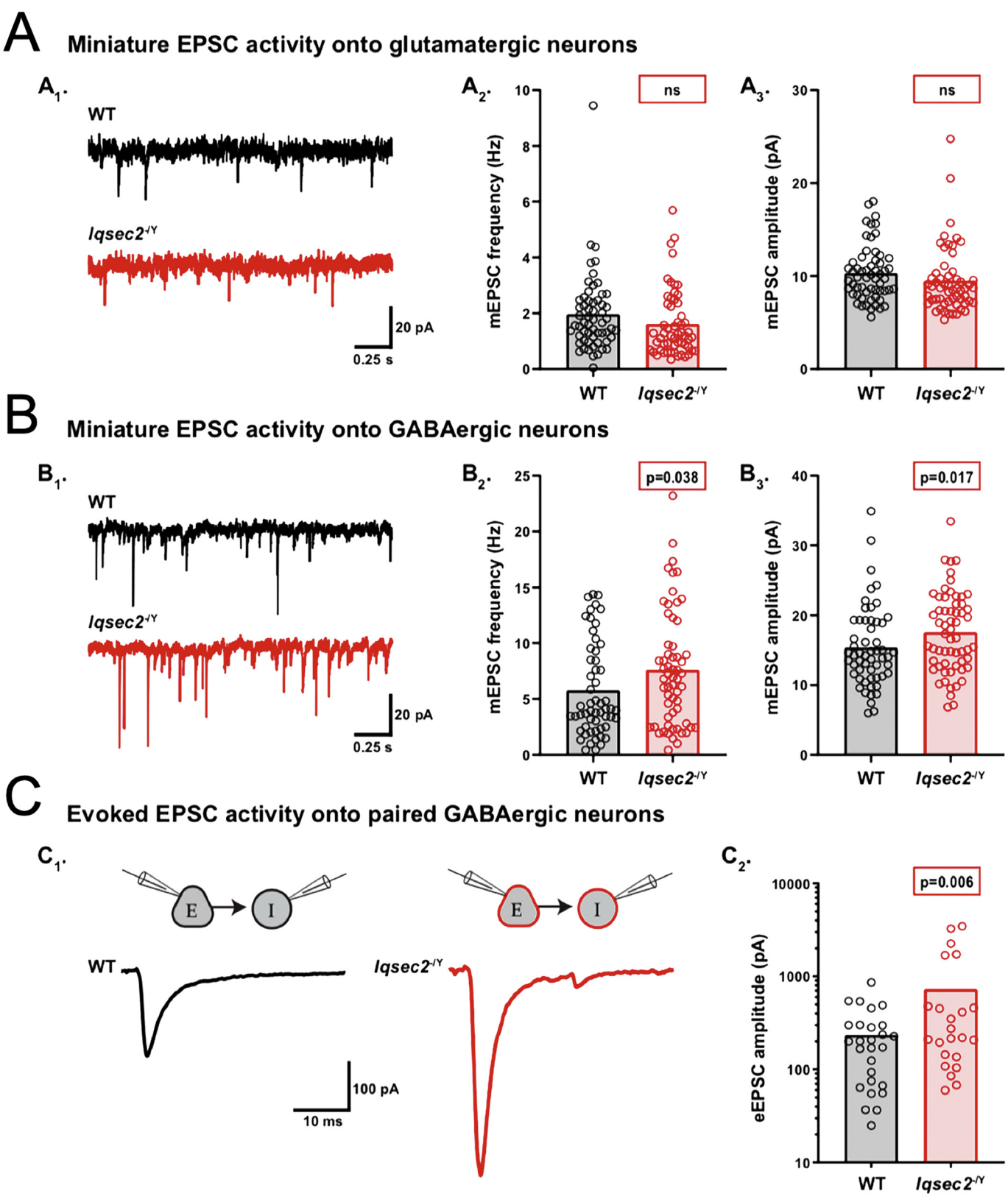

Fig. 4. IQSEC2 loss increases excitatory drive onto GABAergic neurons.

A-C. Using whole-cell, voltage-clamp electrophysiology, spontaneous miniature and evoked activity was recorded from glutamatergic and GABAergic hippocampal neurons derived from wildtype (WT) and *Iqsec2*$^{-/Y}$ mice at days 12–15 *in vitro*. Example traces of miniature EPSC activity onto wildtype (WT) (black) and *Iqsec2*$^{-/Y}$ (red) glutamatergic neurons (A_1) and GABAergic neurons (B_1). Bar graph with overlaid dot plots show that the mEPSC frequency and amplitude onto glutamatergic neurons were both unaltered (A_2 and A_3), whereas onto GABAergic neurons they were both increased (B_2 and B_3), by *Iqsec2* loss. C_1. Example traces of evoked EPSCs onto paired wildtype (WT) (black) and *Iqsec2*$^{-/Y}$ (red) GABAergic neurons. C_2. Bar graphs with overlaid dot plots show that the eEPSC amplitude onto GABAergic neurons was increased by loss of *Iqsec2*. For all graphs, the bars indicate the mean of the data set and each dot represents the mean response from one neuron. All *p*-values were calculated using Generalized Estimating Equations, and significant p-values are indicated in red boxes for each graph (ns indicates $p > .05$).

recorded the eEPSC onto a paired GABAergic neuron (Fig. 4C$_1$), or we stimulated a GABAergic neuron and recorded the eIPSC onto a paired glutamatergic neuron (Supplementary Fig. 4C$_1$). Similar to the mEPSC data, the average amplitude of the EPSCs evoked onto GABAergic neurons was increased in the *Iqsec2*$^{-/Y}$ pairs relative to that of the wildtype pairs (WT: 236 ± 53 pA, *Iqsec2*$^{-/Y}$: 762 ± 184 pA, $p = .006$; Fig. 4C$_{1,2}$). Also, in agreement with the mIPSC data, there was no genotype-dependent difference detected in the eIPSCs onto glutamatergic neurons (WT: 1514 ± 316 pA, *Iqsec2*$^{-/Y}$: 1081 ± 225 pA, $p = .27$; Supplementary Fig. 4C$_{1,2}$). Taken together, these data identify an increase in excitatory synaptic input specifically onto interneurons downstream of IQSEC2 loss, suggesting neuron subtype-specific roles for this PSD protein.

3.7. Loss of Iqsec2 alters the intrinsic electrical properties of GABAergic hippocampal neurons

To determine whether the alterations in synaptic transmission are accompanied by alterations in the intrinsic electrical properties, we performed current-clamp recordings and analyzed passive and active membrane characteristics of glutamatergic and GABAergic neurons from *Iqsec2*$^{-/Y}$ and wildtype hippocampal neuron cultures (DIV12–15). *Iqsec2*$^{-/Y}$ glutamatergic neurons showed no differences in passive or active membrane properties relative to those of wildtype (Supplementary Table 1). However, *Iqsec2*$^{-/Y}$ GABAergic neurons had a more hyperpolarized resting membrane potential, and a lower input resistance with a higher membrane capacitance (WT: −56.7 ± 0.7 mV, *Iqsec2*$^{-/Y}$: −59.1 ± 0.7 mV, $p = .013$; Fig. 5A$_1$, WT: 111.2 ± 7.2 MΩ, *Iqsec2*$^{-/Y}$: 91.1 ± 5.8 MΩ, $p = .030$; Fig. 5A$_2$, and WT: 113.3 ± 5.2 pF, *Iqsec2*$^{-/Y}$: 134.6 ± 6.0 pF, $p = .007$; Fig. 5A$_3$). Frequently, neurons with a hyperpolarized resting membrane potential and lower input resistance also have an increased rheobase, which is the amount of current necessary to stimulate the firing of an action potential (AP). Thus, we next injected increasing amounts of current into the neurons to determine their rheobase. Although the average rheobase of *Iqsec2*$^{-/Y}$ GABAergic neurons appeared to show the predicted increase relative to that of wildtype, the difference was not significant (WT: 245.3 ± 27.4 pA, *Iqsec2*$^{-/Y}$: 319.3 ± 34.6 pA, $p = .094$). Moreover, the AP threshold and amplitude were unaltered by *Iqsec2* loss (WT: −35.5 ± 0.6 mV, *Iqsec2*$^{-/Y}$: −36.1 ± 0.6 mV, $p = .440$; WT: 63.6 ± 1.4 mV, *Iqsec2*$^{-/Y}$: 64.3 ± 1.4 mV, $p = .733$). However, the *Iqsec2*$^{-/Y}$ GABAergic neurons fired APs with narrower half-widths and larger afterhyperpolarizations (AHPs) than wildtype (WT: 0.98 ± 0.04 ms, *Iqsec2*$^{-/Y}$: 0.85 ± 0.03 ms, $p = .009$; Fig. 5B$_{1,2}$, WT: 20.4 ± 0.8 mV, *Iqsec2*$^{-/Y}$: 24.9 ± 0.8 mV, $p < .001$; Fig. 5B$_{1,3}$). Taken together, these data demonstrate profound alterations in multiple intrinsic electrical properties specifically in GABAergic neurons following *Iqsec2* loss, further supporting neuron subtype-specific roles for IQSEC2. Interestingly, several of the observed alterations in *Iqsec2*$^{-/Y}$ GABAergic neurons, including the lower input resistance, narrower AP half-widths, and larger AHPs, are hallmark features of fast-spiking (FS) interneurons, suggesting either an enrichment of FS interneurons, or perhaps, simply an enhancement of an FS-like phenotype due to *Iqsec2* loss.

3.8. Loss of Iqsec2 results in an increase in PV interneurons in adult hippocampus

Together, parvalbumin (PV)- and somatostatin (SST)-expressing interneurons constitute the largest non-overlapping groups of interneurons in cortex and hippocampus. Interneuron maturation is dictated closely by excitatory input during development (Pelkey et al., 2017). Since GABAergic interneurons are impacted upon IQSEC2 loss, we examined expression of these inhibitory cell markers, PV and SST, both temporally at PND16 and PND60, and spatially in cortex and hippocampus. Beginning with mRNA expression we observed a significant increase in PV mRNA expression in the hippocampus of PND60 *Iqsec2*$^{-/Y}$ animals compared with control (*Iqsec2*$^{+/Y}$: 1.005 ± 0.047, *Iqsec2*$^{-/Y}$: 1.547 ± 0.1643, $p = .0225$, Fig. 6A) while the expression of SST across the timepoints and genotypes remained unaltered (Fig. 6A). Since an increase in PV mRNA expression can stem from either a cell intrinsic increase in expression as a response to synaptic activity (Turner et al., 2010) or an increase in number of PV-expressing neurons themselves, we examined PND60 brain sections for PV interneuron expression and found an increased number of PV-expressing cells in the hippocampus of *Iqsec2*$^{-/Y}$ animals (Fig. 6B–D), suggesting that the increase in PV mRNA expression is likely a consequence of an increased number of PV-expressing interneurons. Interestingly, the hippocampus of an outlier PND60 animal (marked in the graphs) showed a robust decrease in PV and SST mRNA expression in both the hippocampus and cortex. Additionally, we carried out morphometric analysis of the dentate gyrus thickness of the PND60 animals and found no difference between the genotypes (Supplementary Fig. 2E), suggesting that the increase in PV cell number occurs without an increase in overall dentate gyrus cell number in adult *Iqsec2*$^{-/Y}$ animals.

Although IQSEC2 is known to densely localize in spines of excitatory neurons, its expression in interneurons was heretofore not described. To further clarify our findings, we also examined IQSEC2 expression in PV-positive cells. Importantly, using DIV14 dissociated hippocampal neuronal cultures, we identified that IQSEC2 is highly expressed in PV-positive interneurons (Fig. 6E). Additionally, PV-positive neurons in brain slices of adult *Iqsec2*$^{+/Y}$ animals were also reactive against the IQSEC2 antibody (Fig. 6E). These findings suggest that developmental loss of IQSEC2 from these FS interneurons may be responsible for alterations in their intrinsic properties.

4. Discussion

De novo and inherited mutations in *IQSEC2* have been identified in multiple patients diagnosed with autism spectrum disorder, intellectual disability, developmental delay, epilepsy and/or epileptic encephalopathy (Mignot et al., 2018; Shoubridge et al., 2019; Radley et al., 2019). Accordingly, *Iqsec2* knockout mice have several neurobehavioral phenotypes anticipated from human clinical features, including spontaneous seizures, developmental delay, hyperactivity and deficits in adult male-female social interactions. In our study we focused on male mice to minimize phenotypic dispersion that results from mosaicism due to random X-inactivation in heterozygous females. We note that several *in vivo* phenotypes are consistent with those reported very recently in an independent *Iqsec2* model that was published while our study was in preparation (Jackson et al., 2019)

Probing further, we noticed several unusual phenotypic features, including relative resistance to both 6 Hz electrically-induced partial or limbic seizures and to pentylenetetrazole-induced tonic-clonic seizures. While these findings are counterintuitive to the occurrence of severe spontaneous seizures, they are nevertheless striking and unique characteristics of the knockout mice offering clues to the underlying cellular and molecular etiology of IQSEC2 loss, in particular by suggesting a focus on the hippocampus and on inhibitory neurotransmission, respectively. Although IQSEC2 is known to be expressed at excitatory synapses and regulates transmission onto excitatory neurons (Murphy, 2006; Brown et al., 2016; Myers et al., 2012), our detailed electrophysiological investigation of hippocampal synaptic transmission showed that loss of IQSEC2 affects excitatory transmission onto GABAergic neurons in a fundamentally different way, and that IQSEC2 is also strongly expressed in parvalbumin-positive hippocampal interneurons - the most abundant type of hippocampal interneuron and tight regulators of excitatory neuron output (Booker and Vida, 2018). Concomitant histological and molecular analysis further compelled our investigations. Specifically in the hippocampus of IQSEC2 deficient mice we observe reactive astrogliosis without overt cell loss. We also observe an age-dependent increase in parvalbumin expression and an

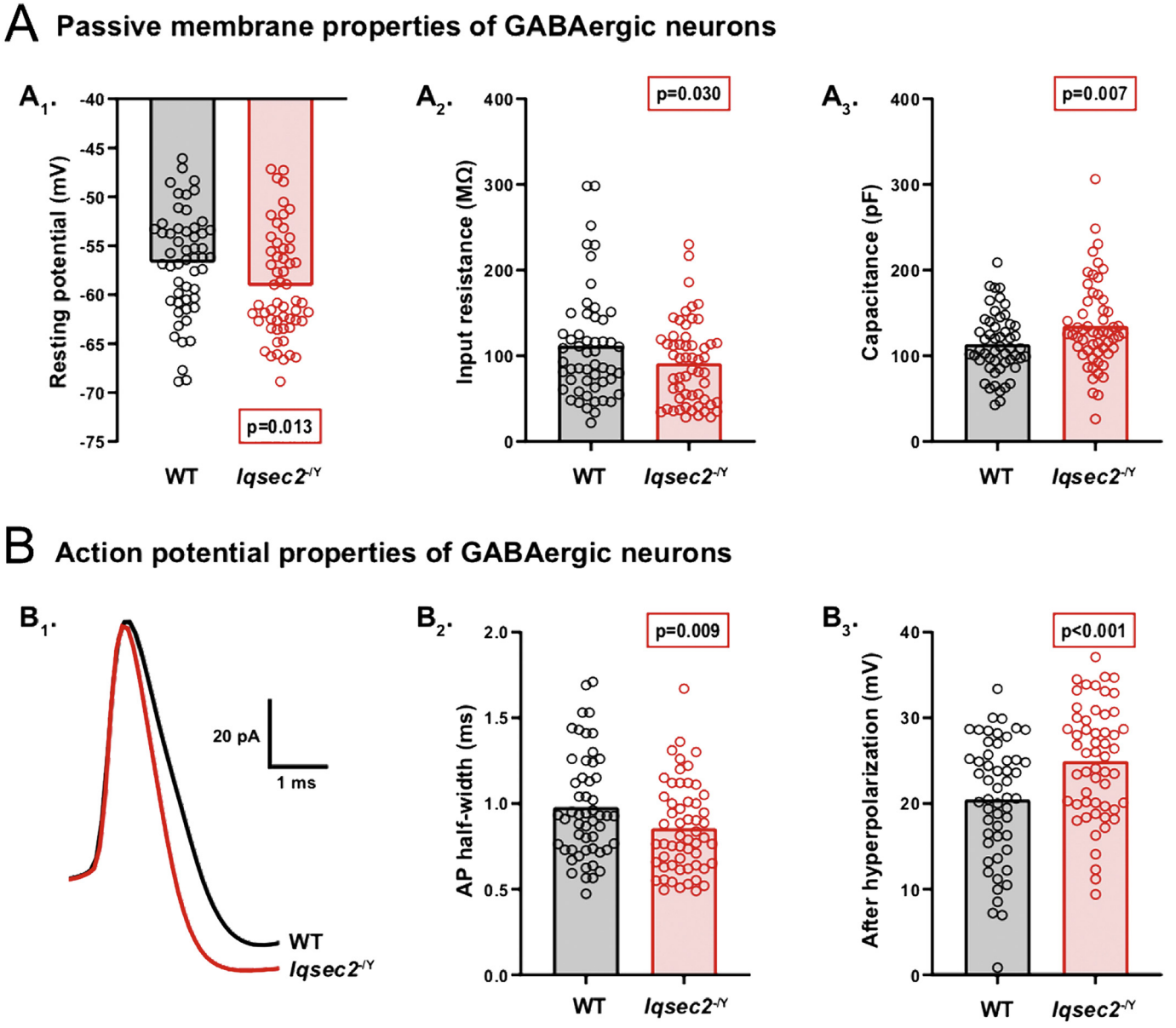

Fig. 5. IQSEC2 loss alters multiple intrinsic electrical properties of GABAergic neurons.
A–B. Using whole-cell, current-clamp electrophysiology, intrinsic electrical properties of GABAergic hippocampal neurons derived from wildtype and *Iqsec2*$^{-/Y}$ mice were assessed at days 12–15 *in vitro*. A. Bar graphs with overlaid dot plots illustrate alterations in passive membrane properties of *Iqsec2*$^{-/Y}$ GABAergic neurons relative to those of wildtype (WT), including a more hyperpolarized resting membrane potential (A_1), a lower input resistance (A_2), and a higher membrane capacitance (A_3). B. Action potential properties of GABAergic neurons were also altered by IQSEC2 loss. B_1. Representative AP traces recorded from wildtype (WT) (black) and *Iqsec2*$^{-/Y}$ (red) GABAergic neurons illustrate the narrower AP half-width (B_2, bar graph with overlaid dot plot) and larger AP afterhyperpolarization (B_3, bar graph with overlaid dot plot) of *Iqsec2*$^{-/Y}$ GABAergic neurons relative to those of wildtype (WT). For all graphs, the bars indicate the mean of the data set and each dot represents the mean response from one neuron. All p-values were calculated using Generalized Estimating Equations, and significant p-values are indicated in red boxes for each graph.

increase in the number of parvalbumin-expressing neurons.

Electrophysiological examination of dissociated hippocampal neurons revealed significant changes at the excitatory synapses onto GABAergic interneurons (but not onto excitatory neurons), namely, an increase in excitatory drive as measured through both miniature and evoked events. Also, only GABAergic hippocampal neurons displayed significant alterations in intrinsic properties. It is known from other studies *in vivo* and *in vitro* that shRNA-mediated loss of IQSEC2 results in increased excitatory cell dendritic branching and spine density (Hinze et al., 2017), factors that could result in an increased dendritic territory for the number of excitatory presynaptic contacts onto interneurons. Our finding that the membrane capacitance, and presumably total membrane area, is increased in *Iqsec2*$^{-/Y}$ GABAergic neurons supports this possibility. The results also suggest the hypothesis that in a hippocampal circuit, the functional consequence of an increased excitatory drive onto interneurons would be a predominantly hyperinhibited network. This hypothesis is consistent with data from Rogers and colleagues (Rogers et al., 2019) who very recently showed a significant decrease in hippocampal synaptic transmission in mutant mice that carry an *Iqsec2* missense mutation.

The medial ganglionic eminence (MGE) produces approximately 60% of all neocortical and hippocampal interneurons and is comprised chiefly of functionally divergent cells types broadly identified by parvalbumin and somatostatin expression (Tricoire et al., 2011; Pleasure

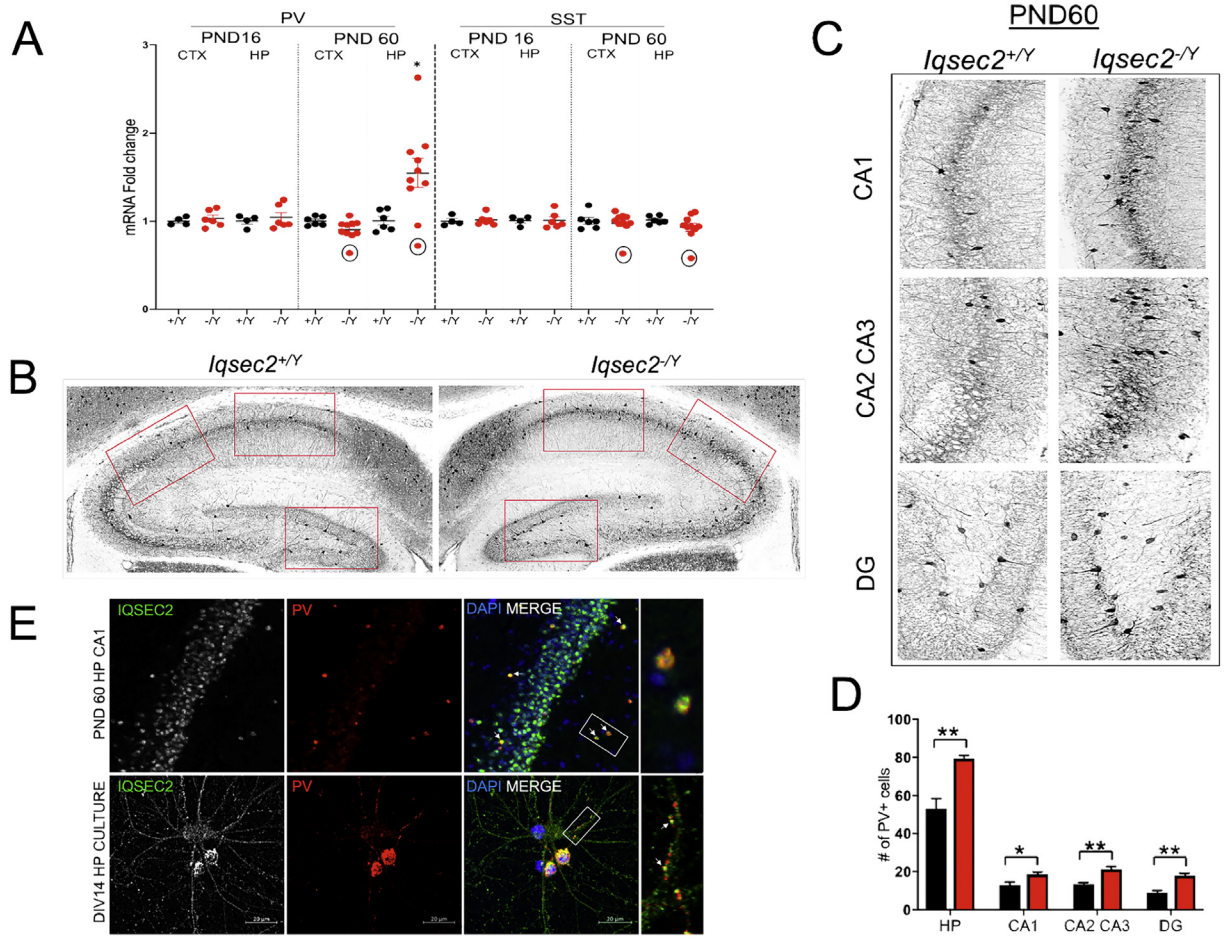

Fig. 6. PV expression is altered in the hippocampus of adult *Iqsec2*$^{-/Y}$ mice.
A. RT-qPCR values from cortical and hippocampal samples of PND14 and PND60 mice representing parvalbumin (*Pvalb*) and somatostatin (*Sst*) mRNA levels. Signals were normalized to *Rpl13* mRNA levels and expressed as fold change compared to *Iqsec2*$^{+/Y}$ mice. Note: the outlier PND60 *Iqsec2*$^{-/Y}$ animal (circled in black in the graphs) with almost a 40% decrease in hippocampal *Pvalb* and *Sst* mRNA compared to control animals showed a similar decrease in *Pvalb* and *Sst* mRNA in the cortex. B. Representative PV immunofluorescence images from hippocampal coronal sections of PND60 *Iqsec2*$^{+/Y}$ and *Iqsec2*$^{-/Y}$ animals. C. Zoomed-in sections indicated by the red boxes in (B) showing PV cells in the CA1, CA2/CA3 and dentate gyrus, respectively. D. Graph shows stereological counts of PV-positive cells in the hippocampus of PND60 animals (4 animals from each genotype, 3 sections each). Student's *t*-test, $*p < .05$, $**p < .01$; error bars indicate ± SEM. E. Confocal images showing double labeling of IQSEC2 and PV in a hippocampal section of a PND60 animal and in dissociated hippocampal cultures at DIV 14. In the hippocampal panel, white arrows in the third section indicate cells which co-labeled for IQSEC2 and PV, while the last section shows a zoomed-in image of the co-labeled cells enclosed by the white box. In the neuron panel, the first section shows endogenous IQSEC2 expression in an excitatory neuron and in PV-expressing interneurons. IQSEC2 is expressed through the entire cell body including protrusions but highly enriched at the postsynaptic sites, evident by the punctate staining expression along the dendrites. Last section shows IQSEC2 and PV co-labeling along dendrites in PV/IQSEC2 positive-interneurons (evident by the co-labeling in the soma) indicating that the two proteins could be co-localized to the same postsynaptic compartments. Scale bar is 20 μm.

et al., 2000; Wonders and Anderson, 2006; Butt et al., 2005). Importantly, the excitatory postsynaptic densities of these MGE derived interneurons differ in molecular composition from the excitatory postsynaptic densities of excitatory and caudal ganglionic eminence (CGE) derived interneurons in that they express calcium permeable GluA1 containing AMPARs but lack receptors containing GluA2 (Akgül and McBain, 2016). Published studies show that while IQSEC2 aids GluA1 internalization (Myers et al., 2012), its overexpression increases GluA2 surface insertion (Brown et al., 2016). Since our results show that loss of IQSEC2 selectively affects excitatory synapses onto GABAergic neurons but not onto excitatory neurons, we hypothesize that the increase in miniature EPSCs upon IQSEC2 loss is being driven by increase in GluA1 expression in MGE derived interneurons. Furthermore, we speculate that even within the MGE population, there may be cell subtypes more vulnerable to IQSEC2 loss. Our electrophysiological recordings show that some altered cell intrinsic properties of GABAergic cells such as lower input resistance, narrower AP half-widths, and larger AHPs resemble features of FS parvalbumin positive cells and our histological data shows a clear increase in the abundance of parvalbumin positive cells in the hippocampus of adult mice. In future studies a conditional knockout approach will help to clarify the cell autonomous role of IQSEC2 in different neuronal subtypes.

It is presently unclear whether the membrane excitability changes in GABAergic neurons are secondary to the increased glutamatergic input or primary drivers of the increased glutamatergic input, or both. The known role of IQSEC2 at the postsynapse suggests that the synaptic changes drive the excitability changes. Other neurodevelopmental disease-causing gene disruptions have also been shown to simultaneously affect membrane excitability and synaptic input suggesting that convergent changes at membranes and synapses (Yi et al., 2016; Tai et al., 2014; Weston et al., 2014) or disruptions in the balance may underlie many disease phenotypes (Antoine et al., 2019). Nevertheless, the data overall strongly implicate inhibitory neurons in the hippocampus as important players of pathogenesis associated with IQSEC2 deficiency.

Several of our observations are consistent with other models of childhood neurodevelopmental diseases in the ASD, ID and epileptic

encephalopathy spectrum. Developmentally increased parvalbumin cell number and parvalbumin mRNA expression was reported in mouse models of Rett Syndrome caused by genetic ablation of *Cdkl5* and *Mecp2* (Zhu and Xiong, 2019; Patrizi et al., 2020; Rudenko et al., 2015; Morello et al., 2018). Excitatory synaptogenesis closely dictates interneuron development (Tremblay et al., 2016; Hu et al., 2017). Overall, parvalbumin expressing cells, compared to other interneuron types, receive over 10-fold more excitatory than inhibitory inputs (Buhl et al., 1996). Additionally, parvalbumin is a calcium-binding albumin protein whose expression in cells is closely regulated by synaptic calcium influx (44). At the excitatory synapse, IQSEC2, which has a calmodulin-binding domain, regulates NMDAR signaling and AMPAR subunit expression, thereby effectively regulating calcium entry into the cell (Rogers et al., 2019; Myers et al., 2012; Brown et al., 2016; Elagabani et al., 2016). IQSEC2 loss might therefore, upset excitatory synaptic activity-induced calcium entry, providing an alternative explanation for the increased parvalbumin expression. Therefore, based on our data, we suggest that a persistent increase in excitatory synaptic input onto these interneurons during development along with compensation for altered calcium dynamics likely results in higher parvalbumin cell expression upon IQSEC2 loss. A small percentage of somatostatin (SST)-producing non-FS cells is also known to express some PV (Maccaferri and McBain, 1995). However, since we did not detect any difference in SST mRNA between the genotypes and timepoints, we conclude that the increased parvalbumin mRNA expression is being driven by an increase in parvalbumin-expressing FS cells.

Fast spiking parvalbumin interneurons mediate feedforward inhibition in the hippocampal and cortical circuits. Since this form of inhibition is strongly effective in preventing the spread of epileptic activity beyond the generation locus, these interneurons are regarded as one of the main obstacles on the pathway to the generation of convulsions (Andreae, 2018). Thus, the sheer increase in number along with an increased excitatory input onto these interneurons may explain the unexpected increased resistance to induced seizures in the mutant animals.

In light of our cellular and electrophysiological observations, an obvious puzzle is how would a hypoexcitable network result in seizure activity? Since the *Iqsec2*$^{-/Y}$ mice die of a lethal seizure, it is tempting to speculate that the abnormally increased excitatory drive onto interneurons may play a role in the preictal transition to seizure activity in a mutant hippocampus. The rationale is that repeated excitation of inhibitory neurons such as that seen with seizure activity would result in switched signs of chloride ion reversal potential, turning GABA release depolarizing from hyperpolarizing (Mackenzie and Maguire, 2015). We also find evidence of hippocampal reactive gliosis in *Iqsec2*$^{-/Y}$ mice suggestive of a region under stress. Although, we did not find any evidence of cell death in adult mice, the increased excitatory drive onto interneurons during development could result in excitotoxicity mediated interneuron cell-death shifting balance to increased excitation. In fact, one knockout animal in our adult mRNA expression profiling group displayed an almost 30% decrease in PV and SST mRNA expression in both the hippocampus and cortex (Fig. 6A). Based on this observation, we predict that recruitment of the cortex by the hippocampus, driven by interneuron cell death, may be the harbinger for seizure activity in these animals.

5. Conclusion

The skewing of E/I balance towards a decreased E/I ratio is indeed increasingly observed in multiple loss-of-function neurodevelopmental disorders in genes encoding neuroligin, β-neurexin, SHANK3, fragile X mental retardation protein (FMRP), and Rett syndrome-associated MeCP2 (Gatto and Broadie, 2010). Importantly, almost all of these genetic models report spontaneous seizure activity. Such a convergence of diverse genetic factors on a few key common features suggests a few impactful mechanisms to maintain status quo. Given the pointed anomalies in hippocampal PV+ interneurons observed here, we expect that continued study of the IQSEC2 model will not only assist in design of therapeutic intervention for IQSEC2 but possibly also in related neurodevelopmental disorders with overlapping pathophysiological signatures.

Acknowledgements

We would like to thank Dr. Randall Walikonis for his generous gift of the IQSEC2 antibody.

Funding

This research was supported by NIH grant R37 NS031348 to Dr. Wayne Frankel at Columbia University Medical Center and NIH grant R01 NS110945 to Matthew Weston at the University of Vermont.

Appendix A. Supplementary data

Supplementary data to this article can be found online at https://doi.org/10.1016/j.nbd.2020.104758.

References

Akgül, Gülcan, McBain, Chris J., 2016. Diverse roles for ionotropic glutamate receptors on inhibitory interneurons in developing and adult brain. J. Physiol. 594 (19), 5471–5490. https://doi.org/10.1113/JP271764.

Andreae, Laura C., 2018. Not just uninhibited: interneurons and seizure onset. Sci. Transl. Med. 10 (468), eaav9143. https://doi.org/10.1126/scitranslmed.aav9143.

Antoine, Michelle W., Langberg, Tomer, Schnepel, Philipp, Feldman, Daniel E., 2019. Increased excitation-inhibition ratio stabilizes synapse and circuit excitability in four autism mouse models. Neuron 101 (4), 648–661.e4. https://doi.org/10.1016/j.neuron.2018.12.026.

Patrizi, Annarita, Awad, Patricia N., Chattopadhyaya, Bidisha, Li, Chloe, Cristo, Graziella Di, Fagiolini, Michela, 2019. Accelerated Hyper-Maturation of Parvalbumin Circuits in the Absence of MeCP2. Cerebral Cortex. https://doi.org/10.1093/cercor/bhz085. Accessed May 21, 2019, published on 30 April.

Baucum, Anthony J., Shonesy, Brian C., Rose, Kristie L., Colbran, Roger J., 2015. Quantitative proteomics analysis of CaMKII phosphorylation and the CaMKII Interactome in the mouse forebrain. ACS Chem. Neurosci. 6 (4), 615–631. https://doi.org/10.1021/cn500337u.

Booker, Sam A., Vida, Imre, 2018. Morphological diversity and connectivity of hippocampal interneurons. Cell Tissue Res. 373 (3), 619–641. https://doi.org/10.1007/s00441-018-2882-2.

Brown, Joshua C., Petersen, Amber, Zhong, Ling, Himelright, Miranda L., Murphy, Jessica A., Walikonis, Randall S., Gerges, Nashaat Z., 2016. Bidirectional regulation of synaptic transmission by BRAG1/IQSEC2 and its requirement in long-term depression. Nat. Commun. 7 (March), 11080. https://doi.org/10.1038/ncomms11080.

Buhl, E.H., Szilágyi, T., Halasy, K., Somogyi, P., 1996. Physiological properties of anatomically identified basket and bistratified cells in the CA1 area of the rat Hippocampus in vitro. Hippocampus 6 (3), 294–305. https://doi.org/10.1002/(SICI)1098-1063(1996)6:3<294::AID-HIPO7>3.0.CO;2-N.

Butt, Simon J.B., Fuccillo, Marc, Nery, Susana, Noctor, Steven, Kriegstein, Arnold, Corbin, Joshua G., Fishell, Gord, 2005. The temporal and spatial origins of cortical interneurons predict their physiological subtype. Neuron 48 (4), 591–604. https://doi.org/10.1016/j.neuron.2005.09.034.

Elagabani, Mohammad Nael, Briševac, Dušica, Kintscher, Michael, Pohle, Jörg, Köhr, Georg, Schmitz, Dietmar, Kornau, Hans-Christian, 2016. Subunit-selective N-methyl-d-aspartate (NMDA) receptor signaling through Brefeldin A-resistant Arf guanine nucleotide exchange factors BRAG1 and BRAG2 during synapse maturation. J. Biol. Chem. 291 (17), 9105–9118. https://doi.org/10.1074/jbc.M115.691717.

Morleo, Manuela, Iaconis, Daniela, Chitayat, David, Peluso, Ivana, Marzella, Rosalia, Renieri, Alessandra, Mari, Francesca, Franco, Brunella, 2008. Disruption of the IQSEC2 transcript in a female with X;autosome translocation t(X;20)(P11.2;Q11.2) and a phenotype resembling X-linked infantile spasms (ISSX) syndrome. Mol. Med. Rep. 1 (1), 33–39.

Frankel, W.N., Taylor, L., Beyer, B., Tempel, B.L., White, H.S., 2001. Electroconvulsive thresholds of inbred mouse strains. Genomics 74 (3), 306–312. https://doi.org/10.1006/geno.2001.6564.

Gatto, Cheryl L., Broadie, Kendal, 2010. Genetic controls balancing excitatory and inhibitory synaptogenesis in neurodevelopmental disorder models. Frontiers in Synaptic Neuroscience 2. https://doi.org/10.3389/fnsyn.2010.00004.

Hinze, S.J., Jackson, M.R., Lie, S., Jolly, L., Field, M., Barry, S.C., Harvey, R.J., Shoubridge, C., 2017. Incorrect dosage of IQSEC2, a known intellectual disability and epilepsy gene, disrupts dendritic spine morphogenesis. Transl. Psychiatry 7 (5), e1110. https://doi.org/10.1038/tp.2017.81.

Hu, Jia Sheng, Vogt, Daniel, Sandberg, Magnus, Rubenstein, John L., 2017. Cortical interneuron development: a tale of time and space. Development 144 (21), 3867–3878.

https://doi.org/10.1242/dev.132852.
Jackson, Matilda R., Loring, Karagh E., Homan, Claire C., Thai, Monica Hn, Määttänen, Laura, Arvio, Maria, Jarvela, Irma, et al., 2019. Heterozygous loss of function of IQSEC2/Iqsec2 leads to increased activated Arf6 and severe neurocognitive seizure phenotype in females. Life Science Alliance 2 (4). https://doi.org/10.26508/lsa.201900386.
Sanda, Masashi, Kamata, Akifumi, Katsumata, Osamu, Fukunaga, Kohji, Watanabe, Masahiko, Kondo, Hisatake, Sakagami, Hiroyuki, 2009. The postsynaptic density protein, IQ-ArfGEF/BRAG1, can interact with IRSp53 through its proline-rich sequence. Brain Res. 1251 (January), 7–15. https://doi.org/10.1016/j.brainres.2008.11.061.
Maccaferri, G., McBain, C.J., 1995. Passive propagation of LTD to stratum Oriens-alveus inhibitory neurons modulates the Temporoammonic input to the hippocampal CA1 region. Neuron 15 (1), 137–145. https://doi.org/10.1016/0896-6273(95)90071-3.
Mackenzie, Gerardo G., Maguire, Jamie L., 2015. Chronic stress shifts the GABA reversal potential in the Hippocampus and increases seizure susceptibility. Epilepsy Res. 109, 13–27. https://doi.org/10.1016/j.eplepsyres.2014.10.003.
Mignot, Cyril, McMahon, Aoife C., Bar, Claire, Campeau, Philippe M., Davidson, Claire, Buratti, Julien, Nava, Caroline, et al., 2018. IQSEC2-related encephalopathy in males and females: a comparative study including 37 novel patients. Genetics in Medicine. https://doi.org/10.1038/s41436-018-0268-1.
Morello, Noemi, Schina, Riccardo, Pilotto, Federica, Phillips, Mary, Melani, Riccardo, Plicato, Ornella, Pizzorusso, Tommaso, Pozzo-Miller, Lucas, Giustetto, Maurizio, 2018. Loss of Mecp2 causes atypical synaptic and molecular plasticity of Parvalbumin-expressing interneurons reflecting Rett syndrome–like sensorimotor defects. ENeuro 5 (5). https://doi.org/10.1523/ENEURO.0086-18.2018.
Murphy, Jessica A., 2006. BRAG1, a Sec7 domain-containing protein, is a component of the postsynaptic density of excitatory synapses. Brain Res. 1120 (1), 35–45. https://doi.org/10.1016/j.brainres.2006.08.096.
Murphy, Jessica A., Jensen, Ole N., Walikonis, Randall S., 2006. BRAG1, a Sec7 domain-containing protein, is a component of the postsynaptic density of excitatory synapses. Brain Res. 1120 (1), 35–45. https://doi.org/10.1016/j.brainres.2006.08.096.
Myers, Kenneth R., Wang, Guangfu, Sheng, Yanghui, Conger, Kathryn K., Casanova, James E., Julius Zhu, J., 2012. Arf6-GEF BRAG1 regulates JNK-mediated synaptic removal of GluA1-containing AMPA receptors: a new mechanism for nonsyndromic X-linked mental disorder. J. Neurosci. Off. J. Soc. Neurosci. 32 (34), 11716–11726. https://doi.org/10.1523/JNEUROSCI.1942-12.2012.
Olson, Heather E., Tambunan, Dimira, LaCoursiere, Christopher, Goldenberg, Marti, Pinsky, Rebecca, Martin, Emilie, Ho, Eugenia, Khwaja, Omar, Walter, E., Poduri, Annapurna, 2015. Mutations in Epilepsy and Intellectual Disability Genes in Patients with Features of Rett Syndrome. American Journal of Medical Genetics. Part A 167A (9). https://doi.org/10.1002/ajmg.a.37132. 2017–25.
Pelkey, Kenneth A., Chittajallu, Ramesh, Craig, Michael T., Tricoire, Ludovic, Wester, Jason C., McBain, Chris J., 2017. Hippocampal GABAergic inhibitory interneurons. Physiol. Rev. 97 (4), 1619–1747. https://doi.org/10.1152/physrev.00007.2017.
Pleasure, S.J., Anderson, S., Hevner, R., Bagri, A., Marin, O., Lowenstein, D.H., Rubenstein, J.L., 2000. Cell migration from the ganglionic eminences is required for the development of hippocampal GABAergic interneurons. Neuron 28 (3), 727–740. https://doi.org/10.1016/s0896-6273(00)00149-5.
Racine, R.J., 1972. Modification of Seizure Activity by Electrical Stimulation. II. Motor Seizure. Electroencephalography and Clinical Neurophysiology 32 (3), 281–294. https://doi.org/10.1016/0013-4694(72)90177–0.
Radley, Jessica A., Rory, B.G.O., Sullivan, Sarah E., Turton, Helen Cox, Vogt, Julie, Morton, Jenny, Jones, Elizabeth, et al., 2019. Deep Phenotyping of Fourteen New Patients with IQSEC2 Variants, Including Monozygotic Twins of Discordant Phenotype. Clinical Genetics. https://doi.org/10.1111/cge.13507. January.
Rogers, Eli J., Jada, Reem, Schragenheim-Rozales, Kinneret, Sah, Megha, Cortes, Marisol, Florence, Matthew, Levy, Nina S., et al., 2019. An IQSEC2 mutation associated with intellectual disability and autism results in decreased surface AMPA receptors. Front. Mol. Neurosci. 12, 43. https://doi.org/10.3389/fnmol.2019.00043.
Sakagami, Hiroyuki, Sanda, Masashi, Fukaya, Masahiro, Miyazaki, Taisuke, Sukegawa, Jun, Yanagisawa, Teruyuki, Suzuki, Tatsuo, Fukunaga, Kohji, Watanabe, Masahiko, Kondo, Hisatake, 2008. IQ-ArfGEF/BRAG1 is a guanine nucleotide exchange factor for Arf6 that interacts with PSD-95 at postsynaptic density of excitatory synapses. Neurosci. Res. 60 (2), 199–212. https://doi.org/10.1016/j.neures.2007.10.013.
Shoubridge, Cheryl, Walikonis, Randall S., Gécz, Jozef, Harvey, Robert J., 2010a. Subtle functional defects in the Arf-specific guanine nucleotide exchange factor IQSEC2 cause non-syndromic X-linked intellectual disability. Small GTPases 1 (2), 98–103. https://doi.org/10.4161/sgtp.1.2.13285.
Shoubridge, Cheryl, Harvey, Robert J., Dudding-Byth, Tracy, 2019. IQSEC2 mutation update and review of the female-specific phenotype Spectrum including intellectual disability and epilepsy. Hum. Mutat. 40 (1), 5–24. https://doi.org/10.1002/humu.23670.
Srivastava, Siddharth, Desai, Sonal, Cohen, Julie, Smith-Hicks, Constance, Barañano, Kristin, Fatemi, Ali, Naidu, SakkuBai, 2018. Monogenic disorders that mimic the phenotype of Rett syndrome. Neurogenetics 19 (1), 41–47. https://doi.org/10.1007/s10048-017-0535-3.
Rudenko, Andrii, Seo, Jinsoo, Hu, Ji, Susan, C. Su, de Anda, Froylan Calderon, Durak, Omer, Ericsson, Maria, Carlén, Marie, Tsai, Li-Huei, 2015. Loss of cyclin-dependent kinase 5 from parvalbumin interneurons leads to hyperinhibition, decreased anxiety, and memory impairment. The Journal of Neuroscience 35 (6), 2372–2383. https://doi.org/10.1523/JNEUROSCI.0969-14.2015.
Tai, Chao, Abe, Yasuyuki, Westenbroek, Ruth E., Scheuer, Todd, Catterall, William A., 2014. Impaired excitability of somatostatin- and Parvalbumin-expressing cortical interneurons in a mouse model of Dravet syndrome. Proc. Natl. Acad. Sci. U. S. A. 111 (30), E3139–E3148. https://doi.org/10.1073/pnas.1411131111.
Shoubridge, Cheryl, Tarpey, Patrick S., Abidi, Fatima, Ramsden, Sarah L., Rujirabanjerd, Sinitdhorn, Murphy, Jessica A., Boyle, Jackie, et al., 2010b. Mutations in the guanine nucleotide exchange factor gene IQSEC2 cause nonsyndromic intellectual disability. Nat. Genet. 42 (6), 486–488. https://doi.org/10.1038/ng.588.
Tremblay, Robin, Lee, Soohyun, Rudy, Bernardo, 2016. GABAergic interneurons in the neocortex: from cellular properties to circuits. Neuron 91 (2), 260–292. https://doi.org/10.1016/j.neuron.2016.06.033.
Tricoire, Ludovic, Pelkey, Kenneth A., Erkkila, Brian E., Jeffries, Brian W., Yuan, Xiaoqing, McBain, Chris J., 2011. A blueprint for the spatiotemporal origins of mouse hippocampal interneuron diversity. J. Neurosci. Off. J. Soc. Neurosci. 31 (30), 10948–10970. https://doi.org/10.1523/JNEUROSCI.0323-11.2011.
Turner, Christopher Paul, DeBenedetto, Danielle, Ware, Emily, Stowe, Robert, Lee, Andrew, Swanson, John, Walburg, Caroline, et al., 2010. Postnatal exposure to MK801 induces selective changes in GAD67 or Parvalbumin. Exp. Brain Res. 201 (3), 479–488. https://doi.org/10.1007/s00221-009-2059-z.
Um, Ji Won, 2017. Synaptic functions of the IQSEC family of ADP-Ribosylation factor guanine nucleotide exchange factors. *Neuroscience Research*, Central synapse, neural circuit and brain function 116 (March), 54–59. https://doi.org/10.1016/j.neures.2016.06.007.
Weston, Matthew C., Chen, Hongmei, Swann, John W., 2014. Loss of MTOR repressors Tsc1 or Pten has divergent effects on excitatory and inhibitory synaptic transmission in single hippocampal neuron cultures. Front. Mol. Neurosci. 7, 1. https://doi.org/10.3389/fnmol.2014.00001.
Wonders, Carl P., Anderson, Stewart A., 2006. The origin and specification of cortical interneurons. Nat. Rev. Neurosci. 7 (9), 687–696. https://doi.org/10.1038/nrn1954.
Yang, Mu, Bozdagi, Ozlem, Scattoni, Maria Luisa, Wöhr, Markus, Roullet, Florence I., Katz, Adam M., Abrams, Danielle N., et al., 2012. Reduced excitatory neurotransmission and mild autism-relevant phenotypes in adolescent Shank3 null mutant mice. J. Neurosci. 32 (19), 6525–6541. https://doi.org/10.1523/JNEUROSCI.6107-11.2012.
Yi, Fei, Danko, Tamas, Botelho, Salome Calado, Patzke, Christopher, Pak, ChangHui, Wernig, Marius, Südhof, Thomas C., 2016. Autism-associated SHANK3 Haploinsufficiency causes Ih Channelopathy in human neurons. Science (New York, N.Y.) 352 (6286), aaf2669. https://doi.org/10.1126/science.aaf2669.
Zhu, Yong-Chuan, Xiong, Zhi-Qi, 2019. Molecular and synaptic bases of CDKL5 disorder. Developmental Neurobiology 79 (1), 8–19. https://doi.org/10.1002/dneu.22639.
Zerem, Ayelet, Haginoya, Kazuhiro, Lev, Dorit, Blumkin, Lubov, Kivity, Sara, Linder, Ilan, Shoubridge, Cheryl, et al., 2016. The molecular and phenotypic Spectrum of IQSEC2-related epilepsy. Epilepsia 57 (11), 1858–1869. https://doi.org/10.1111/epi.13560.